

**Subsurface Radar Sounding of the South Polar Layered Deposits of Mars**

Jeffrey J. Plaut, *et al.*
Science **316**, 92 (2007);
DOI: 10.1126/science.1139672

This copy is for your personal, non-commercial use only.

If you wish to distribute this article to others, you can order high-quality copies for your colleagues, clients, or customers by [clicking here](#).

Permission to republish or repurpose articles or portions of articles can be obtained by following the guidelines [here](#).

The following resources related to this article are available online at www.sciencemag.org (this information is current as of February 21, 2012):

Updated information and services, including high-resolution figures, can be found in the online version of this article at:

<http://www.sciencemag.org/content/316/5821/92.full.html>

This article has been **cited by** 39 article(s) on the ISI Web of Science

This article has been **cited by** 2 articles hosted by HighWire Press; see:

<http://www.sciencemag.org/content/316/5821/92.full.html#related-urls>

Subsurface Radar Sounding of the South Polar Layered Deposits of Mars

Jeffrey J. Plaut,¹ Giovanni Picardi,² Ali Safaeinili,¹ Anton B. Ivanov,¹ Sarah M. Milkovich,¹ Andrea Cicchetti,² Wlodek Kofman,³ Jérémie Mouginot,³ William M. Farrell,⁴ Roger J. Phillips,⁵ Stephen M. Clifford,⁶ Alessandro Frigeri,⁷ Roberto Orosei,⁸ Costanzo Federico,⁷ Iwan P. Williams,⁹ Donald A. Gurnett,¹⁰ Erling Nielsen,¹¹ Tor Hagfors,¹¹ Essam Heggy,⁶ Ellen R. Stofan,¹² Dirk Plettemeier,¹³ Thomas R. Watters,¹⁴ Carlton J. Leuschen,¹⁵ Peter Edenhofer¹⁶

The ice-rich south polar layered deposits of Mars were probed with the Mars Advanced Radar for Subsurface and Ionospheric Sounding on the Mars Express orbiter. The radar signals penetrate deep into the deposits (more than 3.7 kilometers). For most of the area, a reflection is detected at a time delay that is consistent with an interface between the deposits and the substrate. The reflected power from this interface indicates minimal attenuation of the signal, suggesting a composition of nearly pure water ice. Maps were generated of the topography of the basal interface and the thickness of the layered deposits. A set of buried depressions is seen within 300 kilometers of the pole. The thickness map shows an asymmetric distribution of the deposits and regions of anomalous thickness. The total volume is estimated to be 1.6×10^6 cubic kilometers, which is equivalent to a global water layer approximately 11 meters thick.

The polar regions of Mars are covered with extensive finely layered deposits that contain a record of climate variations of an unknown time span (1). Although the precise composition of the deposits is unknown, it is believed that they are predominantly water ice and that they represent the largest known reservoir of H₂O on the planet (2). We applied a technique commonly used to study the interior of ice sheets and glaciers on Earth—radar echo sounding—to study the south polar layered deposits (SPLD) of Mars. We report here on observations of the SPLDs by the Mars Advanced Radar for Subsurface and Ionospheric Sounding (MARSIS) instrument on the Mars Express orbiter. The data were used to characterize the electrical properties of the deposits in order to understand their composition, map the topography of the bed of the deposits, and measure the total volume of the SPLD.

Martian PLD were first identified in orbital images obtained by the Mariner and Viking spacecraft (3–6). They were noted to consist of dozens of layers of contrasting albedo, with thicknesses down to the resolution of the available images (about 10 m). Higher-resolution images acquired by the Mars Orbital Camera on Mars Global Surveyor (MGS) indicated that the scale of layering extends down to the resolution of that camera; that is, a few meters (7). Topographic data obtained by the Mars Orbiter Laser Altimeter (MOLA) on MGS showed that the north PLD (NPLD) and the SPLD are similar in gross morphology and thickness (2). Both the NPLD and SPLD units are roughly domical in shape and about 1000 km across, with maximum relief relative to the surrounding terrain of about 3.5 km. MOLA data were used to estimate the volume of the PLD, which is equivalent to a global layer 16 to 22 m thick (2). Although the relationship of the layering to climate variations is not well understood, it is believed that the rhythmic nature of the deposits is related to oscillations in Mars' orbital parameters (8). The albedo variations among layers are thought to be caused by varying mixtures of ice and dust. The mixing ratio of ice and dust cannot be precisely measured from optical data, but it has been shown that only a small fraction (<10%) of dust is needed to lower the albedo of pure ice to the observed levels (9).

MARSIS is a multifrequency synthetic-aperture orbital sounding radar (10). In its subsurface modes, MARSIS operates in frequency bands between 1.3 and 5.5 MHz, with a 1-MHz instantaneous bandwidth that provides free-space range resolution of approximately 150 m. Lateral spatial resolution is 10 to 30 km in the cross-track direction; and the along-track footprint, narrowed by onboard synthetic-aperture processing, is 5 to 10 km. Processing includes a correction for phase distortion and delay in the ionosphere (11). We

report here on data collected during the southern hemisphere nightside campaign of Mars Express between November 2005 and April 2006. Data were collected during more than 300 orbits, with MARSIS primarily operating in a two-frequency mode using bands centered on 3.0, 4.0, or 5.0 MHz.

The NPLD were observed previously by MARSIS during two orbits in June 2005 (11). The MARSIS signals appeared to penetrate to the base of the deposit, which was estimated to be 1.8 km deep in the thickest area observed, near the periphery of the deposits. The very low attenuation of the MARSIS signals in the NPLD materials suggests that they contain only a few percent dust mixed with pure water ice. The basal interface was seen to remain essentially horizontal beneath the NPLD, showing that flexural downwarping due to the load does not exceed the estimated detection limit of several hundred meters and implying a thick lithosphere in that region of the planet (11).

In a typical MARSIS observation over the SPLD (Fig. 1), the echo from the surface splits into two continuous traces as the spacecraft passes over the margin of the deposits. The surface trace follows a profile expected from MOLA topography. The bright lower trace occurs at a time delay consistent with a continuation of the surrounding surface topography beneath the SPLD, assuming a nominal value of the refractive index of water ice. The lower interface is interpreted as the boundary between the base of the ice-rich SPLD materials and the predominantly lithic substrate. The interface is detected beneath most of the SPLD, although in places it becomes discontinuous, indistinct, or absent. It is generally lower in backscatter intensity than the surface above it, but in places it appears equivalent to or brighter than the surface echo. Propagation of the signal in the SPLD medium can be described with a simple two-layer homogeneous model, using reflection and absorption coefficients that are appropriate for materials expected on Mars. As in the case of the NPLD (11), the strong return from the basal interface indicates very low attenuation values within the SPLD. If the material is assumed to be “dirty” water ice overlying a basaltic substrate, effective loss tangent values between 0.001 and 0.005 are obtained for the SPLD material (12). This corresponds to water ice with a dust contamination of 0 to 10% (13). The general behavior of the surface and subsurface echoes over most of the SPLD is consistent with a composition of water ice that is relatively free of impurities, overlying a typical Martian regolith and crust.

An extended area of unexpectedly bright basal reflections occurs in an area between the thickest part of the SPLD (~3.7 km) and the nearby SPLD margin, from 310° to 0° east longitude (Fig. 1). The returns are often brighter than the surface return, which is not expected for propagation through a lossy medium. Although a strong contrast in dielectric constant at the base

¹Jet Propulsion Laboratory, California Institute of Technology, Pasadena, CA 91109, USA. ²Infocom Department, “La Sapienza” University of Rome, 00184 Rome, Italy. ³Laboratoire de Planétologie de Grenoble, 38041 Grenoble Cedex, France. ⁴NASA/Goddard Space Flight Center, Greenbelt, MD 20771, USA. ⁵Department of Earth and Planetary Sciences, Washington University, St. Louis, MO 63130, USA. ⁶Lunar and Planetary Institute, Houston, TX 77058, USA. ⁷Dipartimento di Scienze della Terra, Università degli Studi di Perugia, 06123 Perugia, Italy. ⁸Istituto di Fisica dello Spazio Interplanetario, Istituto Nazionale di Astrofisica, 00133 Rome, Italy. ⁹Astronomy Unit, School of Mathematical Sciences, Queen Mary University of London, Mile End Road, London E1 4NS, UK. ¹⁰Department of Physics and Astronomy, University of Iowa, Iowa City, IA 52242, USA. ¹¹Max Planck Institute for Solar System Research, 37191 Katlenburg-Lindau, Germany. ¹²Proxemy Research, Laytonsville, MD 20882, USA. ¹³Fakultät fuer Elektrotechnik und Informationstechnik, Technische Universität Dresden, D-01062 Dresden, Germany. ¹⁴Center for Earth and Planetary Studies, National Air and Space Museum, Smithsonian Institution, Washington, DC 20560, USA. ¹⁵Center for Remote Sensing of Ice Sheets, University of Kansas, Lawrence, KS 66045, USA. ¹⁶Fakultät fuer Elektrotechnik und Informationstechnik Ruhr-Universität Bochum, D-44780 Bochum, Germany.

may be responsible, we deem it highly unlikely that liquid water [from basal melting (14)] causes the bright return, because it occurs below thin (as well as thick) sections of the SPLD that are among the coldest places on the surface of Mars. The low attenuation is consistent with very low temperatures throughout

the ice, further arguing against basal melting. Nevertheless, we cannot completely rule out unusual geothermal conditions or an exotic composition of the substrate in these anomalously bright areas.

A pattern of banding commonly occurs between the surface and basal interface traces in

MARSIS radargrams of the SPLD (Fig. 1). The banding consists of bright continuous reflectors, sometimes hundreds of kilometers long, alternating with lower-backscatter bands. The banding is certainly related to the layered structure of the SPLD, possibly due to contrasts in dust content or density, but the precise mechanism that

Fig. 1. (A) MARSIS data from orbit 2753, showing typical features of the SPLD. (B) MOLA topography along the ground track. The lower echo trace (arrows) is interpreted as the SPLD basal interface with the substrate. The basal reflector becomes indistinct at the right of center. The central area shows multiple continuous bands internal to the SPLD, where the estimated SPLD thickness is 1.6 km. (C) MARSIS data from orbit 2682, showing a bright basal reflector (arrow). (D) MOLA topography along the ground track. The reflector extends from the margin of the SPLD (left of center) to below a 3.5-km-thick section of the SPLD. The basal reflector abruptly disappears for unknown reasons. (E) MOLA surface elevations (black line) and MARSIS measured basal elevations (blue symbols), assuming a refractive index of ice. The basal reflector is at a fairly constant elevation between 1000 and 1500 m. The apparent curvature of the reflector in (C) is an artifact of the time representation of the data. The vertical dimension in (A) and (C) is round-trip travel time. See Fig. 2 for the location of ground tracks and the MOLA elevation scale.

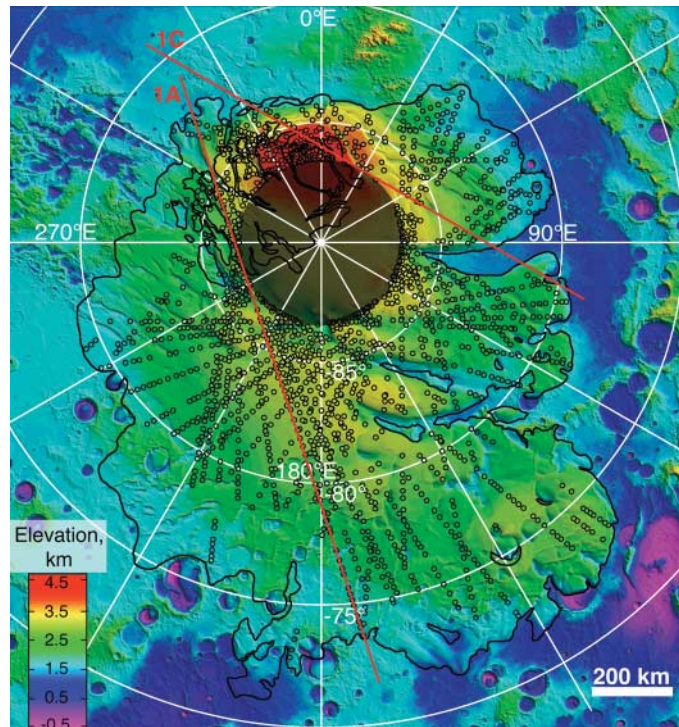
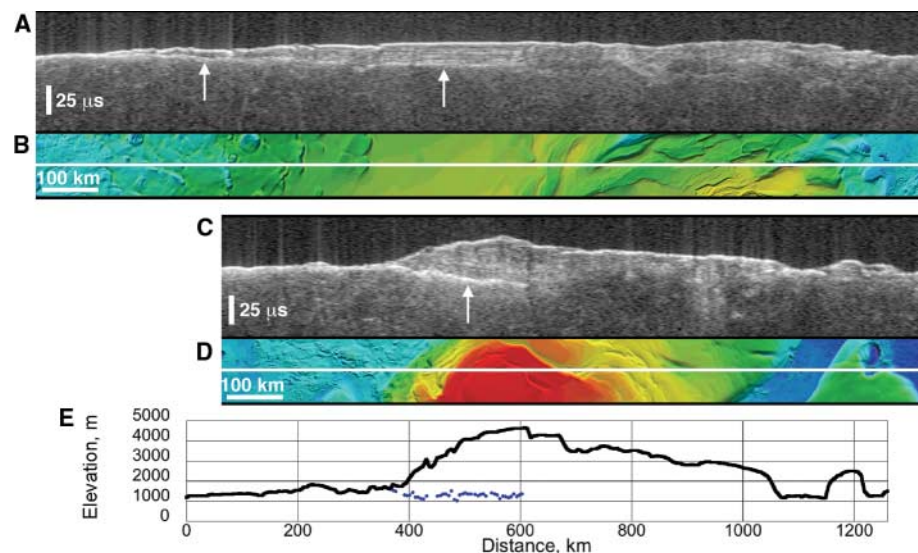
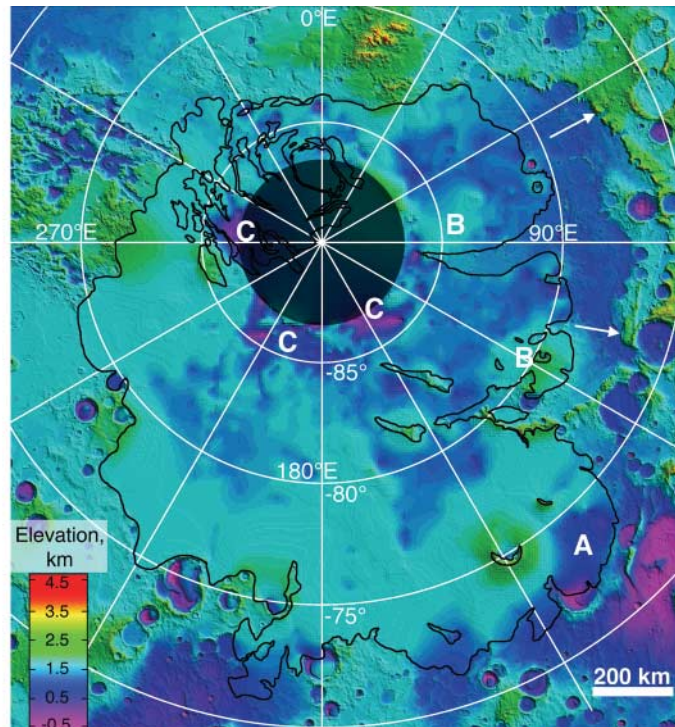


Fig. 2. (left). Topography of the south polar region of Mars from MGS MOLA data, with locations of MARSIS measurements of the SPLD thickness shown as open circles. The SPLD unit as mapped by (15) is outlined in black. Red lines indicate ground tracks of the orbits in Fig. 1. Apparent gaps in coverage are due to the lack of a discernible basal interface, and not to gaps in observations. No MARSIS data are available poleward of



87°S (dark circle in upper center). **Fig. 3** (right). Same as Fig. 2, with topography at the SPLD basal interface shown, based on MARSIS measurements of SPLD thickness. A indicates a depression below a distal SPLD lobe. B indicates relative highs within the remnant Prometheus basin (the basin rim is indicated with arrows). C indicates depressions in the near-polar region.

creates the bands is unknown. The position and brightness of the bands sometimes vary with the frequency of the MARSIS observation, suggesting that the bands may be due to interference effects that depend on the relative scales of the radar wavelength and the internal layering of the SPLD.

Detection of the basal interface below most of the SPLD allows us to generate a map of the topography of this interface and to provide new estimates of the thickness and volume of the SPLD. The methodology used is as follows: The time delay was measured between the peak of the surface reflection and the peak of the last bright continuous reflector, which is assumed to be the basal interface. Over 1800 points from 60 high-quality MARSIS orbits were used. The orbits were chosen to provide coverage that was sufficiently dense to generate medium-resolution maps of basal topography and SPLD thickness. Data from two frequencies were evaluated for most points. All points were verified to be actual subsurface reflectors and not surface “clutter,” using simulations of surface echoes based on MOLA topography (11). The vertical resolution of the data used was about 100 m in ice, with an estimated uncertainty on a given measurement less than 200 m. To convert time delay to depth, we used the refractive index of pure ice with a real dielectric constant of 3. We could reasonably expect this estimate to be off by ± 0.5 , which translates into an additional error in our depth estimate of somewhat less than 10%. Figure 2 shows a map of the locations of the measured points.

To obtain a map of the basal interface, the MARSIS measured elevations of the interface

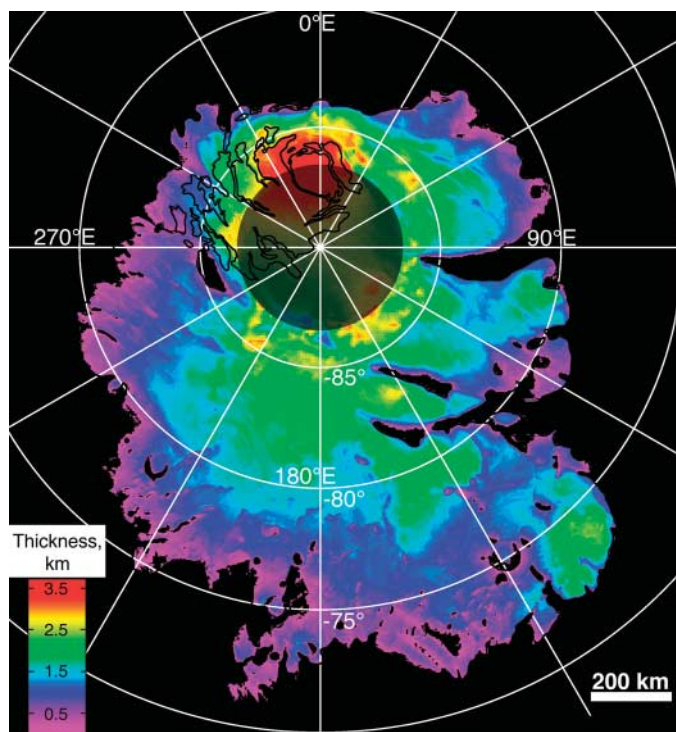
were combined with MOLA elevations along the margin of the SPLD unit as mapped by (15), where the thickness of the unit is considered to be zero. The results of a “natural-neighbor” interpolation (16, 17) of these data are shown in Fig. 3. The map of the sub-SPLD topography is generally consistent with that expected from simple interpolation of MOLA data from the margins of the unit (18). The surface is typically low in relief, with broad areas of higher and lower topography. A pronounced low area is seen near the SPLD margin around 72° to 74°S, 130° to 145°E, and elevated regions within the remnant Prometheus impact basin are seen to continue below the SPLD at 78° to 82°S, 100° to 130°E, and from 70° to 90°E poleward of about 83°S. An unexpected feature of the basal topography is a series of depressions at the highest latitudes (84° to 87°S). These occur discontinuously from longitudes 95° to 295°E. The depressions range in width from 50 to 200 km and reach a depth as much as 1 km below the surrounding sub-SPLD topography. The basal reflection within the depressions is typically dimmer than under the rest of the SPLD. This fact and the position of the depressions in the near-polar areas suggest that there may be processes unique to this sub-SPLD area. The depressions may be the result of differential compaction of megaregolith in response to the SPLD load. Alternatively, they may be a group of buried impact craters or other preexisting topography such as the ~1-km-deep pits (“Cavi”) in the nearby plains. On a regional scale, the basal interface is relatively flat. The lack of evidence of regional downwarping in response to the SPLD load suggests that the

elastic lithosphere in the south polar region is very thick (>150 km), as was inferred for the north polar region (11).

A thickness map of the SPLD was generated by subtracting the elevations of the interpolated basal topography from the high-resolution MOLA surface topography (Fig. 4). The distribution of SPLD thickness reflects the asymmetry of the south polar geology, with the thickest portions offset from the pole near 0°E longitude and the much more areally extensive but thinner portion centered near 180°E. The newly discovered near-polar depressions show clearly as anomalously thick areas, as do several of the distal lobes. The maximum measured thickness is 3.7 ± 0.4 km, under the highest elevations of the SPLD near 0°E. Our estimate of the integrated volume of the entire SPLD is $1.6 \pm 0.2 \times 10^6$ km³ (19). This translates to an equivalent global water layer thickness of 11 ± 1.4 m (assuming an SPLD composition of nearly pure ice) and is within the range estimated by previous workers using MOLA data alone (2, 18, 20). Knowledge of the basal topography now allows us to estimate the volume with a much smaller range of uncertainty.

MARSIS data do not allow us to distinguish a component of CO₂ ice in the SPLD material, but there is no corroborative evidence for such a component. Spectral and albedo observations of the surface of the SPLD indicate an optically thick lag of dust or rocky material, but this layer is “optically” thin at MARSIS wavelengths. Similarly, MARSIS detects no difference in surface or subsurface echoes from areas covered by the residual (“perennial”) CO₂-rich ice unit, which is consistent with recent analyses indicating that it is a deposit no more than a few tens of meters thick (21, 22).

Fig. 4. Map of the SPLD thickness, based on MARSIS measurements and MOLA surface topography. An anomalous thick section appears at lower right (see A in Fig. 3). The thickest areas occur beneath the highest elevations of the SPLD (red areas near the top) and in association with the near-polar depressions (see C in Fig. 3).



References and Notes

- P. C. Thomas, K. Herkenhoff, A. Howard, B. Murray, in *Mars*, H. H. Kieffer *et al.*, Eds. (Univ. of Arizona Press, Tucson, AZ, 1992), pp. 767–795.
- D. E. Smith *et al.*, *J. Geophys. Res.* **106**, 23689 (2001).
- B. C. Murray *et al.*, *Icarus* **17**, 328 (1972).
- J. A. Cutts, *J. Geophys. Res.* **78**, 4231 (1973).
- K. R. Blasius, J. A. Cutts, A. D. Howard, *Icarus* **50**, 140 (1982).
- A. D. Howard, J. A. Cutts, K. R. Blasius, *Icarus* **50**, 161 (1982).
- M. C. Malin, K. S. Edgett, *J. Geophys. Res.* **106**, 23429 (2001).
- O. B. Toon, J. B. Pollack, W. Ward, J. A. Burns, K. Bilski, *Icarus* **44**, 552 (1980).
- H. H. Kieffer, *J. Geophys. Res.* **95**, 1481 (1990).
- G. Picardi *et al.*, in *Mars Express: A European Mission to the Red Planet* [SP-1240, European Space Agency (ESA) Publications Division, European Space Research and Technology Centre, Noordwijk, Netherlands, 2004], pp. 51–69.
- G. Picardi *et al.*, *Science* **310**, 1925 (2005).
- Loss tangent in this context is defined as (ϵ''/ϵ') where ϵ'' and ϵ' are the imaginary and real parts, respectively, of the complex dielectric permittivity.
- E. Heggy *et al.*, in *4th International Conference on Mars Polar Science and Exploration* (Lunar and Planetary Institute, Houston, TX, 2006), abstr. 8105.
- S. M. Clifford, *J. Geophys. Res.* **92**, 9135 (1987).

15. K. Tanaka, E. Kolb, *U.S. Geol. Surv. Open-File Rep. 2005-1271* (2005).
 16. R. Sibson, in *Interpolating Multivariate Data* (Wiley, New York, 1981), pp. 21–36.
 17. We used the natural-neighbor interpolation as implemented in the ArcMap GIS software from ESRI (Redlands, CA). The interpolation applies a weighted moving average and is a preferred method for irregularly distributed data sets (16).
 18. C. Davies, B. A. Murray, J. Byrne, *Eos* **85**, Fall Meeting Supplement, abstr. P13A-0971 (2004).
 19. The error on this estimate includes a 10% uncertainty in refractive index and an additional factor due to gaps in coverage and detectability of the basal interface.
 20. P. M. Schenk, J. M. Moore, *J. Geophys. Res.* **105**, 24529 (2000).
 21. S. Byrne, A. P. Ingersoll, *Science* **299**, 1051 (2003).
 22. J.-P. Bibring *et al.*, *Nature* **428**, 627 (2004).
 23. The authors acknowledge the support of the space agencies of Italy (Agenzia Spaziale Italiana), the United States (NASA), and Europe (European Space

Agency) for the operations of MARSIS and Mars Express. We thank Y. Gim for clutter simulation. Some of the research described in this publication was carried out at the Jet Propulsion Laboratory, California Institute of Technology.

8 January 2007; accepted 27 February 2007
 Published online 15 March 2007;
 10.1126/science.1139672
 Include this information when citing this paper.

Synchronized Oscillation in Coupled Nanomechanical Oscillators

Seung-Bo Shim,* Matthias Imboden, Pritiraj Mohanty†

We report measurements of synchronization in two nanomechanical beam oscillators coupled by a mechanical element. We charted multiple regions of frequency entrainment or synchronization by their corresponding Arnold’s tongue diagrams as the oscillator was driven at subharmonic and rational commensurate frequencies. Demonstration of multiple synchronized regions could be fundamentally important to neurocomputing with mechanical oscillator networks and nanomechanical signal processing for microwave communication.

The concept of synchronized oscillation in coupled systems is pervasive in both nature (1) and human physiology (2). Examples of synchronization include rhythmic blinking of fireflies (3), the activity of pacemaker cells in the sinoatrial node of a human heart (4), and the spin-orbit resonance of the planet Mercury (5). In physical systems, synchronization has been studied for over three centuries, starting

with Huygens’ discovery of the phenomenon in two coupled pendulum clocks (6) and leading to modern-day experiments on coherent radiation in coupled spin-torque nano-oscillators (7, 8) and parametric resonance in mechanical oscillators (9, 10).

Frequency entrainment, a class of synchronization, of coupled micro- and nanomechanical oscillators is of fundamental and technical

interest. A two-oscillator system demonstrates inherently rich linear and nonlinear dynamics, which contrast with its deceptive simplicity (1, 11). After the historical observation of synchronization of two pendulum clocks by Huygens, Appleton (12) and van der Pol (13) showed that the frequency of a triode generator can be entrained, or synchronized, to an external drive; their work was motivated by the potential application in radio communication. The first systematic studies of synchronization in biological systems (and, in particular, human physiology) started with Peskin’s attempt to model self-synchronization of cardiac pacemaker cells to understand the generation of a heartbeat (4). In biological neurocomputing, neural networks show rhythmic behavior, exemplified in many

Department of Physics, Boston University, 590 Commonwealth Avenue, Boston, MA 02215, USA.

*Present address: Center for Strongly Correlated Materials Research and School of Physics and Astronomy, Seoul National University, Seoul, South Korea.

†To whom correspondence should be addressed. E-mail: mohanty@physics.bu.edu

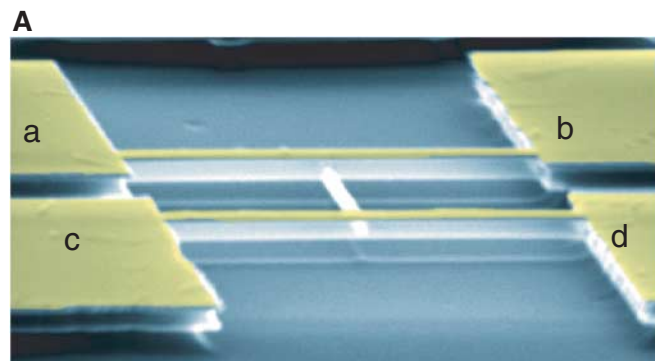
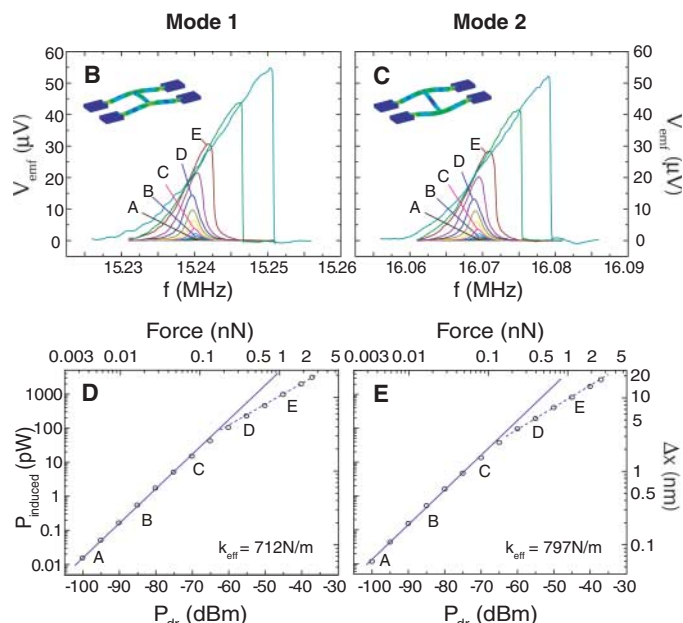


Fig. 1. Device micrograph, magnetomotive characterization, and mode shape. (A) Scanning electron micrograph of the coupled nanomechanical oscillator. Two main beams, each 10 μm in length, are doubly clamped to contact pads a and b and to c and d, respectively. The main beams are mechanically coupled near the center by a 5- μm -long beam. The beams are 500 nm wide and thick. The electrical leads (colored yellow) are selectively deposited such that contacts a and b are electrically isolated from contacts c and d. We observe two separate modes in the coupled nanomechanical resonator, labeled below as mode 1 and mode 2 with resonance frequencies of 15.241 and 16.071 MHz, respectively. (B) Linear and nonlinear response of the device structure in mode 1. The response has Lorentzian shape in the linear regime. Asymmetric responses and hysteresis occur when P_{drive} is greater than -60 dBm (trace D). The inset shows the mode shape from finite element simulation. V_{emf} is the voltage measured by the network analyzer. (C) Linear and nonlinear response of the device structure in mode 2. Nonlinearity commences at similar powers as in the mode 1. (D and E)



Plots of induced power (P_{induced}) as a response of P_{drive} at 5 T. P_{induced} is a measure of the resonant displacement, and P_{drive} corresponds to the driving force. From the log-log plot of driving force versus displacement, we calculate the effective linear-response spring constants $k_{\text{eff}} = 712$ and 797 N/m for modes 1 and 2, respectively. Δx , the central displacement of the beam. See SOM for technical details.